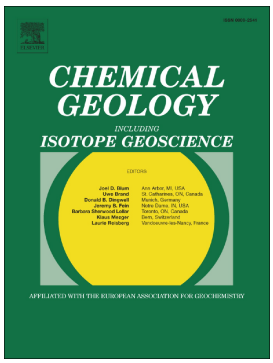

Growth patterns of the topshell Phorcus lineatus (da Costa, 1778) in northern Iberia deduced from shell sclerochronology

Asier García-Escárzaga, Igor Gutiérrez-Zugasti, Bernd R. Schöne, Adolfo Cobo, Javier Martín-Chivelet, Manuel R. González-Morales

PII: S0009-2541(18)30129-3
DOI: doi:10.1016/j.chemgeo.2018.03.017
Reference: CHEMGE 18697

To appear in: *Chemical Geology*

Received date: 17 July 2017
Revised date: 8 February 2018
Accepted date: 8 March 2018

Please cite this article as: Asier García-Escárzaga, Igor Gutiérrez-Zugasti, Bernd R. Schöne, Adolfo Cobo, Javier Martín-Chivelet, Manuel R. González-Morales , Growth patterns of the topshell Phorcus lineatus (da Costa, 1778) in northern Iberia deduced from shell sclerochronology. The address for the corresponding author was captured as affiliation for all authors. Please check if appropriate. Chemge(2018), doi:10.1016/j.chemgeo.2018.03.017

Growth patterns of the topshell *Phorcus lineatus* (da Costa, 1778) in northern Iberia deduced from shell sclerochronology

Asier García-Escárzaga[1,2*], Igor Gutiérrez-Zugasti[1], Bernd R. Schöne[3], Adolfo Cobo[2], Javier Martín-Chivelet[4], Manuel R. González-Morales[1]

[1] Instituto Internacional de Investigaciones Prehistóricas de Cantabria, University of Cantabria. Edificio Interfacultativo, Avda. Los Castros s/n. 39005 Santander, Spain.

[2] Photonic Engineering Group, Department of TEISA, University of Cantabria, Edificio I+D+i de Telecomunicaciones, Avda. Los Castros s/n. 39005 Santander, Spain.

[3] Institute of Geosciences, University of Mainz, Joh.-J.-Becher-Weg 21, 55128 Mainz, Germany

[4] Departamento de Estratigrafía. Facultad de Ciencias Geológicas, Universidad Complutense, e Instituto de Geociencias (CSIC-UCM), Ciudad Universitaria. 28040 Madrid, España.

*Corresponding author. Tel. 34 942202095.

Email address:
a.garcia.escarzaga@gmail.com (A. García-Escárzaga); igorgutierrez.zug@gmail.com (I. Gutiérrez-Zugasti); schoeneb@uni-mainz.de (B.R. Schöne); adolfo.cobo@unican.es (A. Cobo); martinch@ucm.es (J. Martín-Chivelet) moralesm@unican.es (M.R. González-Morales).

Abstract

Combined shell growth pattern and oxygen isotope analysis has become a powerful approach in palaeoclimate and archaeological studies for reconstructing palaeoclimate conditions and littoral exploitation patterns, respectively. Recent investigations have shown that the gastropod *Phorcus lineatus* (da Costa, 1778) forms its shell in conditions of near equilibrium with the oxygen isotope signature of the seawater environment, demonstrating the utility of this species for reconstruction of sea surface temperature and determination of the season of harvest in archaeological studies. In contrast, the shell growth patterns of this species have received virtually no attention despite providing information on the rate and timing of shell growth that is crucial for correctly interpreting environmental proxies derived from shell geochemistry. In this paper, we compare microgrowth patterns and isotopic profiles of four modern individuals of the gastropod *P. lineatus* from northern Iberia to determine the timing and periodicity of subannual growth markers within the shells. Results of this

sclerochronological study showed the presence of two types of growth lines/increments: i) large-scale accretionary units formed with variable periodicity, and ii) small-scale accretionary units formed by micro growth lines and increments determined by semidiurnal tidal cycles. Results suggest that shells grew uninterruptedly during early ontogeny. However, older specimens exhibited growth cessation/slowdown during summer and winter/spring. Therefore, shell growth rate is not only controlled by environmental conditions, but also by ontogenetic age and/or endogenous rhythms. A high correlation was found between seawater temperature derived from shell oxygen isotopes and instrumental seawater temperature (r^2 = 0.88 - 0.98; p-values < 0.0001). This study shows that establishing accurate growth patterns of the topshell *P. lineatus* is essential for correctly reconstructing past seawater temperature conditions in palaeoclimate studies and for determining with higher precision the season(s) when the subfossil shells were collected by humans.

Key words: Sclerochronology, Stable oxygen isotopes, Shells, *Phorcus lineatus*, Growth patterns, Palaeoenvironmental reconstruction, Archaeology.

1. Introduction

Reconstruction of environmental conditions is crucial in geoarchaeological studies to determine the evolution of climate conditions prior to the instrumental era and to better understand human behaviour during prehistoric times. Despite the importance of this topic in current research, it is not a straightforward task, because accurate and precise climate proxies are needed. Stable oxygen isotope ($\delta^{18}O$) data is one of the most used methods to decipher palaeotemperatures (Dorf, 1960; Emiliani et al., 1964; Schöne et al., 2004; Wang et al., 2012) and determine the season when shells were harvested by humans (Burchell et a., 2013a; Colonese et al., 2017; Deith, 1983a; Hausmann and Meredith-Williams, 2016). However, sclerochronological analyses (including geochemical and growth patterns analyses, see Oschmann, 2009 for a definition of the term) have also recently been applied to modern molluscs in order to determine the timing and rate of seasonal shell growth (Carré et al., 2005; Hallmann et al., 2008; 2009; 2013; Schöne et al., 2005a) and to subfossil specimens to reconstruct past environmental conditions (Butler et al., 2013; Hallmann et al., 2011; Lohmann and Schöne, 2013; Reynolds et al., 2017). Furthermore, the number of archaeological investigations that have applied sclerochronological approaches has increased notably during the last decades (Butler and Schöne, 2017; Twaddle et al., 2016), since these

studies enable the determination of the season(s) of capture of the mollusc (Bailey and Craighead, 2003; Deith, 1983b; Gutiérrez-Zugasti, 2009; Milner, 2001) and provide increased accuracy in seasonality estimation by oxygen isotopes, as a consequence of the possibility of a) identifying period of growth cessation, and b) determining the tide type (spring or neap) when the mollusc were harvested (Andrus and Crowe, 2000; Burchell et al., 2013b; Hallmann et al., 2009).

Northern Iberia is one of the key regions for the study of hunter-fisher-gatherer societies from the Upper Palaeolithic and Mesolithic (ca. 45 – 7 ka cal BP) (Fano, 2007; Straus, 2017), thus providing the opportunity for long-term and short-term palaeoclimate studies. Subsistence strategies of past human societies from these time intervals include the collection and consumption of marine resources, such as molluscs, crabs and sea urchins (Álvarez-Fernández, 2011; Gutiérrez-Zugasti, 2011; Gutiérrez-Zugasti et al., 2013; 2016). Sclerochronological analyses can potentially be performed on these shells in order to obtain paleoclimatic and archaeological information. However, before sclerochronology techniques are applied to ancient shells, the proxy should be calibrated using modern representatives of the selected species. Ideally, modern samples should come from the same region where the archaeological shells were collected. One of the most abundant species in the archaeological record of northern Iberia is the topshell *Phorcus lineatus* (da Costa, 1778). This species is especially abundant in archaeological sites dated to the early Holocene (when climatic conditions are assumed to be comparable to the present day, see e.g. Iriarte-Chiapuso et al., 2016; Rofes et al., 2015; Yanes et al., 2012). A closely related species from the Mediterranean, *Phorcus turbinatus*, has received attention as an indicator of palaeotemperatures and to infer the season of shell collection (Colonese et al., 2009; Mannino et al., 2008; 2011; Prendergast et al., 2016). The first isotopic studies of modern and archaeological shells of *P. lineatus* from the European Atlantic façade provided oxygen isotope records that were related to seasonal variations in seawater temperature (Deith, 1983a; Deith and Shackleton, 1986; Mannino and Thomas, 2007; Mannino et al., 2003). Recently, a systematic calibration of oxygen isotopes in their role as a palaeothermometer using modern specimens of *P. lineatus* from northern Iberia (Fig. 1) was published (Gutiérrez-Zugasti et al., 2015). The calibration included closer monitoring of environmental variables than in previous studies, a larger sample size, a higher sampling resolution and seawater monitoring. The study concluded that the topshell *P. lineatus* forms its shells in conditions of near equilibrium with the oxygen isotopic composition of the surrounding

seawater environment, and demonstrated that the topshells can be used as reliable recorders of sea surface temperatures (Gutiérrez-Zugasti et al., 2015).

However, shell growth patterns of *P. lineatus* have received almost no attention. Mollusc shells usually slow down or even stop growing at different times of the year and do so for various different reasons (e.g. extreme temperatures, storms, spawning, etc.) (Schöne, 2008). During growth cessation environmental signals are not recorded by the shell, and therefore actual seawater temperatures can be under- and/or overestimated. For this reason, understanding shell growth patterns is crucial not only for an accurate reconstruction of seawater temperatures, but also for the interpretation of the season of collection of archaeological shells. In this paper, we combine oxygen isotope profiles and microgrowth lines/increment analyses in order to determine growth patterns of topshells of the species *P. lineatus* from northern Iberia. With this aim, a total of four shell oxygen isotope profiles are compared with shell microgrowth lines and increments to determine the seasonal timing and rate of shell growth. Then, we discuss the possible causes of growth cessations, the accuracy of seawater temperature reconstruction, and the implications of the results for paleoclimatic and archaeological studies.

2. Background

2.1 Study area: geographical, environmental and marine conditions

Coastal areas of northern Iberia, the so-called Cantabrian coast (Fig. 1), are defined by oceanic, humid and temperate climatic conditions, exhibiting four well differentiated seasons throughout the year. According to the Köppen climate classification, these conditions can be defined as mesothermal, more precisely as a Cfp type (temperate without dry season and with warm summer). The mean annual land surface temperature (~15-16 ºC) is higher than expected for this latitude (ca. 43ºN), because of the influence of the North Atlantic Current. The coldest month is January with an average temperature of 9-10ºC and the warmest month is August with 20-22ºC. Mean annual rainfall during 1981-2010 exceeded 1100 mm. From October to April the area receives more than 100 mm per month (with 160 mm November is the wettest month). Rainfall decreases considerably from May to September (with 50 mm July is the driest month), coinciding with the warmer months (Source: National Meteorology Agency, http://www.aemet.es). The higher rainfall is a result of the Foehn Effect, a well-

defined effect in areas located to the lee side of a mountain range (Usabiaga et al., 2004). The Cantabrian Sea (southern Bay of Biscay) represents a boundary between subtropical and boreal conditions in the Eastern Atlantic. The study area is characterised by semidiurnal tides. The minimum and maximum tidal amplitude during neap and spring tides are ca. 1 m and ca. 5 m, respectively (Source: http://www.puertos.es). The seawater temperature in the central part of the Cantabrian region (data for Santander) follows a seasonal warming and cooling pattern, ranging from ~23 to ~11ºC (Source: Spanish Institute of Oceanography).

2.2 Biology and ecology of *Phorcus lineatus* (da Costa, 1778)

The topshell *P. lineatus* (Fig. 2a) is a marine gastropod that inhabits the intertidal rocky shores (Crothers, 2001). The mobility of this taxon seems be scarce (generally lower than 1 metre per tidal cycle) and shows a marked homing behaviour, i.e. a preference for returning to their habitat zones (Diez-Urrutia, 2014). Its geographical distribution ranges from southern Morocco to southern Britain and Ireland (Donald et al., 2012; Kendall, 1987; Lewis, 1964), although during the last decades a rapid extension of the northern limit has been documented as a consequence of global climate warming (Mieszkowska et al., 2007). The length of *P. lineatus* rarely exceeds 35 mm (Regis, 1972) and its longevity is generally less than ten years (Crothers, 1994). Previous studies using different techniques, such as petrographic microscopy, scanning electron microscopy (SEM) and x ray diffraction (XRD), have identified that *P. lineatus* exhibits an outer calcitic shell layer and an inner aragonitic layer (Gutiérrez-Zugasti et al., 2015; Mannino and Thomas, 2007; Mannino et al., 2003) (Fig. 2b). *P. lineatus* becomes adult and sexually mature when its length is greater than 9-10 mm, i.e., during the second year of life (Bode et al., 1986; Desai, 1966; Williams, 1965). In northern Iberia, the spawning or breeding stage occurs from June-July to September and gonadal development from November to May-June (Bode et al., 1986; Lombas et al., 1984).

3. Materials and methods

3.1 Shell samples

Four specimens of *P. lineatus* were collected alive from the high shore of a moderately exposed rocky intertidal zone at Langre Beach (Cantabria, Spain) on 22 April 2012 (LANO-65 and LANO-66) and 1 October 2012 (LANO-61 and LANO-63). The

specimens were sacrificed immediately after collection by immersion in boiling water, thus avoiding further deposition of calcium carbonate. In order to remove organic matter from the shells they were treated with 30 vol% H_2O_2 for 48 h. Subsequently shells were air-dried at ambient temperature (Colonese et al., 2009; Gutiérrez-Zugasti et al., 2015). The height (or length) and maximum diameter (or width) of each mollusc shell were measured using a digital calliper to the nearest 0.01 mm. The shells were partially coated with a protective layer of metal epoxy and sectioned in two halves along the growth axis of the last whorl (producing one half with the apex and another with the aperture) using a Buehler Isomet low-speed saw (Fig. 2a).

3.2 Sampling procedures for oxygen isotopes

Carbonate powder samples were taken directly from the aragonite layer of one of the halves (the one with the apex) of each specimen using a dentist´s microdrill with a 0.3 mm drill bit coupled to a microscope. Sampling spots were ca. 0.3 mm apart from each other. A total of 39, 30, 36 and 36 powder samples were taken sequentially from the edge throughout the last whorl of specimens LANO-61, LANO-63, LANO-65 and LANO-66, respectively. Carbonate samples weighing between 100 and 200 µg and were analysed in an IRMS Thermo Scientific MAT 253 coupled to a Kiel device at the Complutense University of Madrid (Spain). Each powder sample was dissolved with concentrated phosphoric acid at 70 ºC. Isotopic ratios were calibrated against the NBS-19 standard ($\delta^{18}O$ = -1.91‰) and the results are reported as $\delta^{18}O$ (‰) relative to the Vienna Pee Dee Belemnite (VPDB) standard. The analytical error of the instrument was better than ±0.03 ‰.

3.3 Thick-sections and sclerochronology

A 2 mm-thick section was cut from the second half of each shell (the one with the aperture) in order to be used for growth pattern analysis (Fig. 2b). These data were later used to temporally align the isotope sample spots. The sections were glued onto a glass slide and the surface was ground on glass plates (600 and 800 SiC grit powder) and polished with 1 µm diamond suspension. Following Schöne et al. (2005b), polished sections were immersed in Mutvei´s solution for 20 min to increase the visibility of the growth lines and increments (Fig. 2c). Finally, the thick-sections were studied with sectoral dark field illumination under a Leica S8APO stereoscopic microscope (8-50x magnification) and with reflected light under a

Leica DM 2500M optical microscope (50-100x magnification) at the IIIPC – University of Cantabria (Spain), coupled in both cases to a Leica MC190HD digital camera (10MP).

To temporally align the isotope sample spots, we followed the method by Schöne et al. (2007). First, reference marks were made on the half section used for carbonate sampling and then on the thick-section of each shell with the aim of locating the actual position of each $\delta^{18}O_{shell}$ sample in relation to the different microgrowth lines and increments. Then, assuming that microgrowth lines and increments recorded at the shell edge (last portion of growth) represented the dates of collection (October 1st for LANO-61 and LANO-63 and April 22th for LANO-65 and LANO-66), the $\delta^{18}O_{shell}$ values were placed into a precise temporal context considering that each tidal cycle (12.4 hours) resulted in the formation of one microgrowth line and one microgrowth increment. Fortnightly (spring tide) bundles of growth lines were also considered for temporal alignment. Finally, each $\delta^{18}O_{shell}$ value was assigned to a variable number of days according to the number of tidal cycles covered by each sample spot.

3.4 Instrumental data

Daily instrumental seawater temperature (T_{meas}) data was provided by the Spanish Institute of Oceanography (Santander, Cantabria) (Fig. 1), which is located close to Langre beach (< 10 km), the shell collection area. The conditions of the sea are similar in both areas, with no influence of continental runoff or sea currents with different salinity. Data on oxygen isotope composition of seawater ($\delta^{18}O_{water}$) was taken from previous studies in the same area covering the period between October 2011 and October 2012 (Gutiérrez-Zugasti et al., 2015, 2017). In these studies, a total of 20 seawater samples were collected throughout a year at the harvest site of the mollusc shells studied here, i.e., Langre Beach. These investigations reported a maximum, minimum and mean value of 0.55‰, 1.19‰ and 0.9‰, respectively, showing a range of 0.64‰. These results suggest fully marine conditions at the location where the shell samples were collected, with only minor changes linked to the hydrological balance during the year. The information about tide cycles and levels was obtained from the website of the Santander Port (Source: http://www.puertosantander.es) and the WXTide32 computer program (www.wxtide32.com).

3.5 Predicted $\delta^{18}O_{shell}$ and oxygen isotope-derived temperatures ($T_{\delta 18O}$)

$\delta^{18}O_{shell}$ values for each day were predicted from daily T_{meas} and $\delta^{18}O_{water}$ in order to test whether temporal alignment of $\delta^{18}O_{shell}$ profiles was correctly performed. To estimate $\delta^{18}O_{water}$ values for those days without data, an interpolation between two known values was applied. For the period prior to October 2011 no data on $\delta^{18}O_{water}$ were available, so the average annual value of the period October 2011 – October 2012 (0.9 ‰) was used. Predicted $\delta^{18}O_{shell}$ was calculated using the water-aragonite fractionation factor obtained by Kim et al. (2007) for synthetic aragonite (Eq. 1). Likewise, reconstructed $T_{\delta 18O}$ was calculated using Eq. (1).

$$1000\ln\alpha = 17.88 * (10^3 / T) - 31.14 \quad (1)$$

where T corresponds to instrumental seawater temperature (T_{meas}) in Kelvin and α is the fractionation between water and aragonite described by the equation:

$$\alpha = 1000 + \delta^{18}O_{shell}\,(\text{SMOW \%}) / 1000 + \delta^{18}O_{water}\,(\text{SMOW \%}) \quad (2)$$

3.6 Measuring the time of *P. lineatus* immersion

To measure the time of immersion of the higher zone of the intertidal area (where this species is found) both during spring and neap tides an experimental programme was developed. Firstly, a reference mark was made on one rock clearly located in the higher zone and then its time of immersion during a spring and neap tide was manually measured.

4. Results

4.1 Shell size

The average length and diameter of the shells used in this study was 15 mm and 16,2 mm, respectively (Table 1). However, the shells collected in autumn showed smaller sizes than the shells collected in spring (Table 1).

4.2 Oxygen isotopes

$\delta^{18}O_{shell}$ of all specimens showed seasonal variations throughout the isotopic profiles, exhibiting robust and well-defined patterns (Fig. 3). The minimal and maximal values documented exhibited some differences between specimens, which is reflected in the standard deviation (SD) of ±0.19 for maximal and ±0.32 for minimal values (Table 1). The specimen collected in October (LANO-61 and LANO-63) showed nearly identical $\delta^{18}O_{shell}$ values at the shell edge (0.90‰) (Fig. 3a-b). The same applies to the $\delta^{18}O_{shell}$ values of the last formed shell material of the specimens collected in April (LANO-65 and LAN-66: 1.71‰ and 1.76‰, respectively) (Fig. 3c-d). The distances between the shell edge and contemporaneous extreme values (i.e., minimal and maximal) differed among specimens (Fig. 3). For example, in the case of the specimens collected in April (Fig. 3a-b), the minimum value of each shell was located at a different distance. Moreover, LANO-63 did not show the annual maximum exhibited by LANO-61 because the distance covered by our sampling strategy was not sufficient.

4.3 Microgrowth increments and temporal alignment

Mutvei-stained cross-sections revealed distinct growth patterns of different orders (Fig. 4), i.e. large- and small-scale accretionary units. (1) Large-scale accretionary units (Fig. 4a-d) are prominent lines, which likely correspond to periods of shell growth cessation/slowdown (Fig. 4a-d). Among these, two different typologies were recognised: very marked growth lines in which the calcite penetrated into the aragonite layer (Fig. 4a-b), and thinner and brighter lines, which do not show any abrupt disruption in the growth patterns (Fig. 4c-d). (2) Small-scale accretionary units (Fig. 4e) are defined by bundles composed of microgrowth lines (darker surfaces) and increments (lighter surface) of micrometric scale. Bundles with strongly developed lines and narrow increments alternated periodically with weakly developed lines and broader increments. One microgrowth increment and one microgrowth line represents a tidal cycle (circatidal increment) and couplets of two microgrowth increments and two lines represent a lunar day (circalunidian increment) (Fig. 4e). The shells analysed here did not show prominent fortnightly lines. However, the calcium carbonate deposited during spring tides exhibited narrow microgrowth lines and broad increments, whereas during the neap tides it showed broader microgrowth lines and narrower increments. Following this approach, the number of circalunidian growth increments corresponded very closely to the expected number of lunar days per each fortnightly period (Fig. 5a). Moreover, the temporal alignment of $\delta^{18}O_{shell}$ using daily and fortnightly

increments, described in detail for the last third of LANO-63 life span (Fig. 5b), reported a significant correlation (r^2 = 0.84, p-value < 0.0001) with predicted $\delta^{18}O_{shell}$. The high correlation has confirmed that temporal alignment was accurately performed and growth increment periodicity correctly deciphered.

Subsequently, and after the periodicity of accretionary units was properly decoded, all isotopic data from shells LANO-61, LANO-63, LANO-65 and LANO-66 were temporally aligned with shell growth patterns and then compared to predicted $\delta^{18}O_{shell}$. The measured and predicted isotope data were in excellent agreement (Fig. 6a-d) as supported by the high correlations (r^2> 0.90, p-values < 0.0001). Each isotope sample covered a different amount of time, ranging from one to 20 days. The mean temporal resolution of each carbonate sample observed in the smaller specimens (LANO-61 and LANO-63) was 4 and 2.6 days, respectively. However, the mean temporal resolution from larger shells (LANO-65 and LANO-66), was 6.3 and 6.1 days per sample, respectively. Larger specimens showed the lowest resolution (20 days per sample) during winter 2010. The smallest time averaging occurred in samples from shell portions formed during late summer and autumn.

Once the temporal alignment was performed, daily growth increment widths, growth rates and periods of growth cessation/slowdown were studied. The daily amount of growth (Fig. 7) for each shell was calculated from the distance between two carbonate samples (600 µm) and the number of days determined through growth pattern analysis (Fig. 6). Growth rates were found not to be constant throughout the life time and they also varied among specimens. For example, LANO-61 (Fig. 7a) and LANO-63 (Fig. 7b) grew uninterruptedly throughout the last whorl, covering the two extreme seasons (summer and winter) in the case of LANO-61, but only the summer in the case of LANO-63. LANO-61 grew fastest during summer, whereas LANO-63 grew at the highest rates in autumn. However, LANO-65 (Fig. 7c) and LANO-66 (Fig. 7d) exhibited lower overall growth rates and their growth record covered a longer time interval, i.e., two winters and one summer. As indicated by growth pattern analysis, these two shells stopped growing during two months in summer (ca. July 15 to September 15), but also during a shorter period (2-3 weeks) in winter (January-February) and spring (April-May). The reported growth cessation/slowdown of these shells is well defined in the shell cross-sections by the absence of the expected number of fortnightly increments (considering 6/7 spring tides per season) and by the existence of different types of

growth checks coincident with more extensive growth slowdowns/stoppages in summer (Fig. 4a-c) or winter and spring (Fig. 4b-d).

4.4 Reconstructed seawater temperatures

$T_{\delta 18O}$ closely reflects T_{meas} (Fig. 8), showing high correlation ($r^2 > 0.88$, p-values < 0.0001). The overlap between the two variables is especially significant in smaller specimens, collected in October 2012 (Fig. 8a-b; $r^2 = 0.96 - 0.98$, p-values < 0.0001). The slight decrease in the correlation coefficient obtained from the shells collected in April 2012 (Fig. 8c-d; $r^2 = 0.88 - 0.90$, p-values < 0.0001) is probably due to lower $T_{\delta 18O}$ than T_{meas} from September 2010 to November 2010. The difference between $T_{\delta 18O}$ and T_{meas} from each specimen is always less than ±0.8 ºC and rarely exceeded ±1 ºC (Table 2). Minimum annual sea water temperatures are well represented (Table 3), e.g., the reconstructed winter temperatures matched the instrumental temperature (11ºC) very well. An exception can be seen in the case of LANO-63, because the sequence obtained from this shell does not cover the winter (2011/2012) prior to collection. However, maximum $T_{\delta 18O}$ (22.5ºC for LANO-61 and 21.6ºC for LANO-63 and 19.5ºC for LANO-65 and LANO-66) does not match the maximum T_{meas} (23.1ºC for LANO-61 and LANO-63 and 21.5ºC for LANO-65 and LANO-66).

4.5 Time of *P. lineatus* immersion

The results obtained showed that the reference mark made was submerged during 5 hours during a tidal cycle (period between a low tide and the next low tide = ~12.4 h) occurring during a spring tide dated on June 25th 2017 (high tide at 6:27 pm, with a maximum height of 5.03 m). On the other hand, the same reference mark was submerged during a total time of 3 hours throughout a tidal cycle during a neap tide dated on July 2nd 2017 (high tide at 12:34 pm, with a maximum height of 3.75 m). Therefore, the species studied here were submerged for longer (40%) periods during spring tides than during neap tides.

5. Discussion

5.1 Shell oxygen isotopes

Oxygen isotope profiles exhibited a strong sinusoidal pattern (Fig. 3). These variations are mainly related to seasonal changes in seawater temperature, since seawater oxygen isotope data showed fully marine conditions, with only minor changes in the hydrological balance throughout the year. This temperature dependence was previously demonstrated for *P. lineatus* in previous isotopic studies on this species (Gutiérrez-Zugasti et al., 2015; Mannino et al., 2003). In fact, the average and extreme isotope values reported here (Table 1) are similar to those of other shells collected at the same location (Gutiérrez-Zugasti et al., 2015) and also to those reported by other scholars for the Cantabrian region (Deith, 1983a; Deith and Shackleton, 1986; Mannino et al., 2003). Even though the maximal and minimal $\delta^{18}O_{shell}$ values are similar to those previously published data, differences between specimens have been observed. In particular, specimen LANO-63 showed a much lower maximum $\delta^{18}O_{shell}$ value than other specimens. The minima documented from LANO-65 and LANO-66 are higher than those obtained from the other two shells (Table 1). The high correlation observed between measured and predicted $\delta^{18}O_{shell}$ was similar to that reported in previous studies of *P. lineatus* (Gutiérrez-Zugasti et al., 2015) and suggests that in this species, shell calcium carbonate was deposited under conditions of (or close to) isotopic equilibrium with the ambient water.

5.2 Subdaily, daily and fortnightly increments

Mutvei-stained cross-sections enabled the periodicity of the different accretionary units deposited by *P. lineatus* over their life span to be deciphered. Large-scale accretionary units (Fig. 4a-b) coincided with more extensive growth slowdowns/stoppages in summer and winter/spring. Small-scale accretionary units exhibit a circatidal periodicity, depositing a microgrowth increment during mollusc submersion and a microgrowth line when molluscs were air exposed. This tide-controlled shell growth is typically observed in the intertidal and subtidal species (Gutiérrez-Zugasti et al., 2017; Milano et al., 2017; Reza Mirzae et al., 2014; Schöne, 2008). Bundles with strongly developed lines and narrow increments alternated periodically with weakly developed lines and broader increments in a fortnightly growth pattern, which is explained by the habitat of this species. The topshell *P. lineatus* inhabits the medium-high intertidal zone, where theoretically the shells are submerged (and growing) for a longer time during spring tides than during neap tides. In order to verify this hypothesis an experimental programme was developed and the results obtained have suggested that the shells studied here were submerged (and growing) for a longer time during the spring tides

than during neap tides, confirming thus, that the broader increments and narrower microgrowth lines correspond to spring tides.

5.3 Annual growth patterns and ontogeny

Molluscs usually slow down or even stop the precipitation of shell calcium carbonate for different reasons (Schöne, 2008), e.g., thermal tolerance (Salas et al., 2014; Surge et al., 2013), reproductive cycle (Sato, 1995), ontogeny (Román-González et al., 2017) or food supply (Joubert et al., 2014). Considering that seawater temperatures are not recorded during growth interruptions, understanding the seasonal variations of shell growth rates is crucial to properly comprehend environmental and archaeological information retrieved from ancient mollusc shells. In the case of *P. lineatus*, the growth interruptions observed in winter do not seem to be caused by thermal stress because the lowest annual temperatures were recorded in two shells (Fig. 8a and 8c-d). However, they could be linked to the reproductive cycle. According to previous studies conducted by other scholars on the biology of *P. lineatus* (Bode et al., 1986; Lombas et al., 1984), the biometric data of all specimens analysed here indicated that they were sexually mature. Two main processes are related to the reproductive cycle, gametogenesis, which occurs in *P. lineatus* from northern Iberia between November and May-June (Bode et al., 1986; Lombas et al., 1984) and spawning, which occurs from June-July to September (Bode et al., 1986; Lombas et al., 1984). Data presented here suggest that gametogenesis might be responsible for growth cessation in winter and spring. Growth cessation provoked by gonadal development has also been documented in other species such as *Spisula solidissima* (Jones, 1980) and *Macoma balthica* (Cardoso et al., 2013), although not in *P. turbinatus* from the Mediterranean, whose maximum growth rate was documented precisely during gametogenesis (Mannino et al., 2008; Prendergast et al., 2013). On the other hand, a growth cessation was observed in LANO-65 and LANO-66 during two months in summer (ca. July 15 to September 15). Although the timing of the stoppage of growth in summer coincided with spawning, it may be related to thermal stress because the release of gametes into seawater requires less energy than gonadal development (Mannino et al., 2008). The summer growth cessation caused by thermal stress has been reported for *P. turbinatus* in southern Italy (Colonese et al., 2009; Mannino et al., 2008), although not in other areas of the Mediterranean such as Malta (Prendergast et al., 2013) and Libya (Prendergast et al., 2016).

Therefore, two different timings of shell growth patterns were observed in *P. lineatus*: (1) LANO-61 and LANO-63 grew uninterruptedly year-round exhibiting higher growth rates during the summer, and probably autumn (this part of the year is barely represented in the studied shell portion) (Fig. 7a-b). This finding is in agreement with previously published data (Gutiérrez-Zugasti et al., 2015). (2) LANO-65 and LANO-66 also showed higher growth rates in autumn, although growth ceased for two months in summer and for shorter periods in winter and spring (Fig. 7c-d). The observed differences are likely linked to shell size (Table 1). Previous studies on the biology of *P. lineatus* from southern Britain reported a correlation between shell size and ontogenetic age (Crothers, 1994; Kendall, 1987). The different shell sizes recorded here indicate that all shells were not at the same stage of life. LANO-65 and LANO-66 were probably ontogenetically older than LANO-61 and LANO-63 (Table 1), and so they experienced periods of growth cessation/slowdown during the time periods of maximum stress. The absence of annual growth checks (or rings) in the Cantabrian latitude (Williamson and Kendall, 1981) and the difficulty of taking calcium carbonate samples from shell edges to shell apex (generally very eroded) have precluded the accurate determination of the ontogenetic age of the specimens used in this study. However, the biological data available for this species suggest a significant correlation between shell size and ontogenetic age. Moreover, the data obtained in this study also seem to confirm this idea, since the growth rates of older/larger shells (LANO-65 and LANO-66) during summer/autumn 2010 (i.e., ca. 18 months before their collection) is very similar to that reported for the younger specimens during those months previous to their collection (Fig. 7). This comparison between growth rates of smaller and larger shells showed that specimens were at a different stage of life when they were collected and also, a clear reduction of the growth rates as a consequence of the ontogeny. This reduction in the growth rates as a consequence of ontogeny, has been documented by other scholars for shorter-lived species (Mannino et al., 2008; Schöne et al., 2003; Schöne, 2008).

5.4 Implication for palaeoclimatological and archaeological studies

$T_{\delta 18O}$ reconstructed from $\delta^{18}O_{shell}$ data followed T_{meas} very closely (Fig. 8), with the exception of values from September to November 2010 in the case of LANO-65 and LANO-66 (Fig. 8c-d). This discrepancy may be explained by the decline in the mean salinity value from September to November 2010. A decrease of 10% in the seawater salinity with respect to the annual average (35 PSU) was recorded in these months (Source: Spanish Institute of

Oceanography). This change could have influenced the isotopic composition of the seawater, provoking thus a reduction of $\delta^{18}O_{water}$ values (and temperature). Despite the offsets documented in these two shells, $T_{\delta 18O}$ exhibited a strong correlation with T_{meas} in the four shells (Fig. 8; r^2 = 0.88 - 0.98, p-values < 0.0001), in agreement with correlations previously published for this species (Gutiérrez-Zugasti et al., 2015). Likewise, $T_{\delta 18O}$ covered the T_{meas} range during shell growth very well, with a mean offset of less than 0.8 ºC (Table 2). Therefore, the data presented here confirm that the topshell *P. lineatus* is an adequate palaeothermometer in northern Iberia. However, the shells do not record the temperature throughout the entire year (Table 3) because shell growth ceases in ontogenetically older specimens during the warm season.

In archaeology, deciphering the season of shell collection is not only crucial to understanding subsistence strategies, but it is also key for the interpretation of human settlement patterns and site use. Moreover, the combined analysis of shell oxygen isotopes and growth patterns can provide important insights to better understand human behaviour. Identifying whether the collection was performed during spring or neap tides is important for the interpretation of shell collection strategies and resource management (Hallmann et al., 2009). Shell collection during spring tides can indicate knowledge of tidal cycles. During spring tides, low intertidal areas are easily accessible providing a broad range of resources. Given that collection in these areas is usually more dangerous than in higher zones of the intertidal area, this behaviour has usually been interpreted as an indicator of intense exploitation of shellfish (Gutiérrez-Zugasti, 2011; Gutiérrez-Zugasti et al., 2013). At this study location (with its characteristic tidal patterns), broad microgrowth increments close to the shell edge of *P. lineatus* suggest that collection would have taken place during spring tides (Fig. 5a), while the presence of narrow microgrowth increments would indicate harvest during neap tides. Considering that the morphology of the coastline in the Cantabrian region, during the Prehistoric time was very similar to today (rocky exposed shores) (Gutiérrez-Zugasti, 2009; Gutiérrez-Zugasti et al., 2013), sclerochronological analyses on *P. lineatus* sections can be easily applied to subfossil shells recovered from archaeological sites, in order to identify the tide features when molluscs were collected.

6. Conclusions

Understanding the timing and rate of shell growth is crucial for the accurate interpretation of environmental and cultural information recorded in geochemical data of the shells. Following previous sclerochronological studies, we have shown that the growth patterns of the gastropod *P. lineatus* are tidal related, showing circatidal and circalunidian increments, and narrower and broader increments during neap and spring tides, respectively. This study showed that two smaller shells grew uninterruptedly year-round, but growth cessation was observed in two shells larger than 17 mm. Accordingly, ontogenetically older specimens are less tolerant to environmental and physiological stress (temperature, gametogenesis). The ontogenetic reduction in growth rate implies that younger shells better represent the annual range of seawater temperatures, and therefore smaller/younger shells should be used for paleoclimate reconstructions.

However, mature specimens can still be used to estimate the season of collection, which is relevant to better understanding human behaviour in coastal areas during prehistoric times. The data presented here suggest that even these specimens are able to record the coldest temperature during winter and at least 35% of the thermal variability during summer. Moreover, the results obtained here also have implications for the interpretation of coastal resource management strategies, because the dataset demonstrates that sclerochronology is able to provide information about the type of the tide when the shells were collected (spring or neap tide).

Acknowledgments

This research was performed as part of the project TRACECHANGE: Tracing Climatic Abrupt Change Events and their Social Impact during the Late Pleistocene and Early Holocene (15-7 ky calBP) (2014-2016) (HAR2013-46802-P), funded by the Spanish Ministry of Economy and Competitiveness, MINECO. AGE was funded by the University of Cantabria through a predoctoral grant (no code available). IGZ was also supported by the Juan de la Cierva Research Programme (grant number JCI-2012-12094) funded by the MINECO. We thank the Fishing Activity Service of the Cantabrian Government for the authorization to collect modern *Phorcus lineatus* specimens, and the Aquaculture Facility of Santander's Oceanographic Centre for providing sea surface temperatures and sea surface salinity. We also thank the Universidad de Cantabria (UC), Johannes Gutenberg Universität (JGU) Mainz, Universidad Complutense de Madrid (UCM), Instituto Internacional de

Investigaciones Prehistóricas de Cantabria (IIIPC) and Grupo de Ingeniería Fotónica (GIF) for providing support. We would also like to thank José Miguel López-Higuera (GIF), David Cuenca-Solana (IIIPC), Roberto Suárez-Revilla (IIIPC), Lucía Agudo Pérez (IIIPC) and Elena Manteca-Rivera (UC). We also thank the three anonymous reviewers for their useful comments.

References

Álvarez-Fernández, E., 2011. Humans and marine resource interaction reappraised: Archaeofauna remains during the late Pleistocene and Holocene in Cantabrian Spain. Journal of Anthropological Archaeology, 30(3): 327-343.

Andrus, C.F.T., Crowe, D.E., 2000. Geochemical Analysis of *Crassostrea virginica* as a Method to Determine Season of Capture. Journal of Archaeological Science, 27(1): 33-42.

Bailey, G.N., Craighead, A.S., 2003. Late Pleistocene and Holocene coastal paleoeconomies: a reconsideration of the molluscan evidence from Northern Spain. Geoarchaeology An International Journal, 18(2): 175-204.

Bode, A., Lombas, I., Anadon, N., 1986. Preliminary studies on the reproduction and population dynamics of *Monodonta lineata* and *Gibbula umbilicalis* (Mollusca, Gastropoda) on the central coast of Asturias (N. Spain). Hydrobiologia, 142(1): 31-39.

Burchell, M., Cannon, A., Hallmann, N., Schwarcz, H.P., Schöne, B.R., 2013a. Inter-site variability in the season of shellfish collection on the central coast of British Columbia. Journal of Archaeological Science, 40(1): 626-636.

Burchell, M., Cannon, A., Hallmann, N., Schwarcz, H., Schöne, B., 2013b. Refining estimates for the season of shellfish collection on the Pacific northwest coast: applying high-resolution stable oxygen isotope analysis and sclerocrhoronology. Archaeometry, 55(2): 258-276.

Butler, P.G., Schöne, B.R., 2017. New research in the methods and applications of sclerochronology. Palaeogeography, Palaeoclimatology, Palaeoecology, 465, Part B: 295-299.

Butler, P.G., Wanamaker Jr, A.D., Scourse, J.D., Richardson, C.A., Reynolds, D.J., 2013. Variability of marine climate on the North Icelandic Shelf in a 1357-year proxy archive based on growth increments in the bivalve Arctica islandica. Palaeogeography, Palaeoclimatology, Palaeoecology, 373: 141-151.

Cardoso, J.F.M.F., Santos, S., Witte, J.I.J., Witbaard, R., van der Veer, H.W., Machado, J.P., 2013. Validation of the seasonality in growth lines in the shell of *Macoma balthica* using stable isotopes and trace elements. Journal of Sea Research, 82: 93-102.

Carré, M., Bentaleb, I., Blamart, D., Ogle, N., Cardenas, F., Zevallos, S., Kalin, R. M., Ortlieb, L., Fontugne, M., 2005. Stable isotopes and sclerochronology of the bivalve *Mesodesma donacium*: Potential application to Peruvian paleoceanographic reconstructions. Palaeogeography, Palaeoclimatology, Palaeoecology, 228(1–2): 4-25.

Colonese, A.C., Troelstra, S., Ziveri, P., Martini, F., Lo Vetro, D, Tommasini, S., 2009. Mesolithic shellfish exploitation in SW Italy: seasonal evidence from the oxygen isotopic composition of *Osilinus turbinatus* shells. Journal of Archaeological Science, 36(9): 1935-1944.

Colonese, A.C., Clemente, I., Gassiot, E., López-Sáez, J.A., 2017. Oxygen isotope seasonality determinations of marsh clam shells from prehistoric shell middens in Nicaragua, Climate Change and Human Responses. Springer, pp. 139-152.

Crothers, J.H., 1994. Student investigations on the populations structure of the common topshells, *Monodonta lineata*, on the Gore, Somerset. Field Studies, 8: 337-355.

Crothers, J.H., 2001. Common topshells: An introduction to the biology of *Osilinus lineatus* with notes on other species in the genus. Field Studies, 10: 115-160.

Deith, M., 1983a. Seasonality of shell collecting, determined by oxygen isotope analysis of marine shells from Asturian sites in Cantabria. In: Grigson, C., Clutton-Brock, J. (Eds.), Animals and Archaeology. BAR International Series, Oxford, pp. 67-76.

Deith, M.R., 1983b. Molluscan calendars: The use of growth-line analysis to establish seasonality of shellfish collection at the Mesolithic site of Morton, Fife. Journal of Archaeological Science, 10(5): 423-440.

Deith, M., Shackleton, N.J., 1986. Seasonal exploitation of marine molluscs: oxygen isotope analysis of shell from La Riera cave. In: Straus, L.G., Clark, G.A. (Eds.), La Riera cave. Stone age hunter-gatherer adaptations in northern Spain. Arizona State University, Tempe, pp. 199-313.

Desai, B.N., 1966. The Biology of *Monodonta Lineata* (da Costa). Journal of Molluscan Studies, 37(1): 1-17.

Díez-Urrutia, C., 2014. Distribución espacial de *Osilinus* spp. (Mollusca: Gasteropoda) en función de la amplitud de marea y el oleaje. Anales Universitarios de Etología, 8: 7-14.

Donald, K.M., Preston, J., Williams, S.T., Reid, D.G., Winter, D., Álvarez, R., Buge, B., Hawkins, S.J., Templado, J., Spencer, H.G., 2012. Phylogenetic relationships elucidate colonization patterns in the intertidal grazers *Osilinus* Philippi, 1847 and *Phorcus* Risso, 1826 (Gastropoda: *Trochidae*) in the northeastern Atlantic Ocean and Mediterranean Sea. Molecular phylogenetics and evolution, 62(1): 35-45.

Dorf, E., 1960. Climate changes of the past and present. American Scientist, 48(3): 341-364.

Emiliani, C., Cardini, L., Mayeda, T., McBurney, C.B.M., Tongiorgi, E., 1964. Palaeotemperature analysis of marine molluscs (food refuse) from the site of Arene Candide cave, Italy and the Haua Fteah cave, Cyrenaica. In: Craig, H., Miller, S.L., Wasserburg, G.J. (Eds.), Isotopic and Cosmic Chemistry. North Holland, Amsterdam pp. 133-166.

Fano, M.Á., 2007. Las sociedad del Paleolítico en la región cantábrica. Kobie, Serie Anejos (8), Bilbao.

Gutiérrez Zugasti, I., 2009. La explotación de moluscos y otros recursos litorales en la región cantábrica durante el Pleistoceno final y el Holoceno inicial. Publican, Ediciones Universidad de Cantabria, Santander.

Gutiérrez-Zugasti, I., 2011. Coastal resource intensification across the Pleistocene–Holocene transition in Northern Spain: Evidence from shell size and age distributions of marine gastropods. Quaternary International, 244(1): 54-66.

Gutiérrez-Zugasti, I., Cuenca-Solana, D., Rasines del Río, P., Muñoz, E., Santamaría, S., Morlote, J.M., 2013. The role of shellfish in hunter–gatherer societies during the Early Upper Palaeolithic: A view from El Cuco rockshelter, northern Spain. Journal of Anthropological Archaeology, 32(2): 242-256.

Gutiérrez-Zugasti, I., García-Escárzaga, A., Martín-Chivelet, J., González-Morales, M.R., 2015. Determination of sea surface temperatures using oxygen isotope ratios from *Phorcus lineatus* (Da Costa, 1778) in northern Spain: Implications for paleoclimate and archaeological studies. The Holocene, 25(6): 1002-1014.

Gutiérrez-Zugasti, I., Tong, E., García-Escárzaga, A., Cuenca-Solana, D., Bailey, G.N., González-Morales, M.R., 2016. Collection and consumption of echinoderms and crustaceans at the Mesolithic shell midden site of El Mazo (northern Iberia): Opportunistic behaviour or social strategy? Quaternary International, 407: 118-130.

Gutiérrez-Zugasti, I., Suárez-Revilla, R. Clarke, L.J., Schöne, B.R., Bailey, G.N., González-Morales, M.R., 2017. Shell oxygen isotope values and sclerochronology of the limpet *Patella vulgata* Linnaeus 1758 from northern Iberia: Implications for the reconstruction of past seawater temperatures. Palaeogeography, Palaeoclimatology, Palaeoecology, 475: 162-175.

Hallmann, N., Schöne, B.R., Strom, A., Fiebig, J., 2008. An intractable climate archive — Sclerochronological and shell oxygen isotope analyses of the Pacific geoduck, *Panopea abrupta* (bivalve mollusk) from Protection Island (Washington State, USA). Palaeogeography, Palaeoclimatology, Palaeoecology, 269(1): 115-126.

Hallmann, N., Burchell, M., Schöne, B.R., Irvine, G.V., Maxwell, D., 2009. High-resolution sclerochronological analysis of the bivalve mollusk *Saxidomus gigantea* from Alaska and British Columbia: techniques for revealing environmental archives and archaeological seasonality. Journal of Archaeological Science, 36(10): 2353-2364.

Hallmann, N., Schöne, B.R., Irvine, G.V., Burchell, M., Cokelet, E.D., Hilton, M.R., 2011. An improved understanding of the Alaska Coastal Current: The application of a bivalve growth-temperature model to reconstruct freshwater-influenced paleoenvironments. PALAIOS, 26(6): 346-363.

Hallmann, N., Burchell, M., Brewster, N., Martindale, A., Schöne, B.R., 2013. Holocene climate and seasonality of shell collection at the Dundas Islands Group, northern British Columbia, Canada-A bivalve sclerochronological approach. Palaeogeography, Palaeoclimatology, Palaeoecology, 373: 163-172.

Hausmann, N., Meredith-Williams, M., 2016. Seasonal Patterns of Coastal Exploitation on the Farasan Islands, Saudi Arabia. The Journal of Island and Coastal Archaeology: 1-20.

Iriarte-Chiapusso, M.J., Muñoz Sobrino, C., Gómez-Orellana, L., Hernández-Beloqui, B., García-Moreiras, I., Fernández Rodriguez, C., Heiri, O., Lotter, A.F., Ramil-Rego, P., 2016. Reviewing the Lateglacial–Holocene transition in NW Iberia: A palaeoecological approach based on the comparison between dissimilar regions. Quaternary International, 403: 211-236.

Jones, D.S., 1980. Annual cycle of Shell growth increment formation in two continental shelf bivalves and its paleoecologic significance. Paleobiology, 6; 331-340.

Joubert, C., Linard, C., Le Moullac, G., Soyez, C., Saulnier, D., Teaniniuraitemoana, V., Ky, C.L., Gueguen, Y., 2014. Temperature and food influence shell growth and mantle gene expression of shell matrix proteins in the pearl oyster Pinctada margaritifera. PLoS ONE, 9(8): e103944.

Kendall, M.A., 1987. The age and size structure of some northern populations of the trochid gastropod *Monodonta lineata*. Journal of Molluscan Studies, 53: 213-222.

Kim, S.T., O'Neil, J.R., Hillaire-Marcel, C., Mucci, A., 2007. Oxygen isotope fractionation between synthetic aragonite and water: Influence of temperature and Mg^{2+} concentration. Geochimica et Cosmochimica Acta, 71(19): 4704-4715.

Lewis, J.R., 1964. The ecology of rocky shores. English Universities Press, London.

Lohmann, G., Schöne, B.R., 2013. Climate signatures on decadal to interdecadal time scales as obtained from mollusk shells (*Arctica islandica*) from Iceland. Palaeogeography, Palaeoclimatology, Palaeoecology, 373: 152-162.

Lombas, I., Bode, A., Anadon, N., 1984. Estudio del ciclo reproductor de *Gibbula umbilicalis* y *Monodonta lineata* en Asturias (N de España), Actas do 4º Simposio Iberico de Estudos do Benthos marinho, Lisboa, pp. 103-114.

Mannino, M.A., Thomas, K.D., 2007. Determining the season of collection of inter-tidal gastropods from $\delta^{18}O$ analysis of shell carbonates: modern analogue data and "internal analysis" of data from archaeological shells In: Milner, N., Craig, O.E., Bailey, G.N. (Eds.), Shells Middens in Atlantic Europe Owbow books Oxford, pp. 111-122.

Mannino, M.A., Spiro, B.F., Thomas, K.D., 2003. Sampling shells for seasonality: oxygen isotope analysis on shell carbonates of the inter-tidal gastropod *Monodonta lineata* (da Costa) from populations across its modern range and from a Mesolithic site in southern Britain. Journal of Archaeological Science, 30(6): 667-679.

Mannino, M.A., Thomas, K.D., Leng, M.J., Sloane, H.J., 2008. Shell growth and oxygen isotopes in the topshell Osilinus turbinatus: resolving past inshore sea surface temperatures. Geo-Marine Letters, 28(5-6): 309-325.

Mannino, M.A., Thomas, K.D., Leng, M.J., Di Salvo, R., Richards, M.P., 2011. Stuck to the shore? Investigating prehistoric hunter-gatherer subsistence, mobility and territoriality in a Mediterranean coastal landscape through isotope analyses on marine mollusc shell carbonates and human bone collagen. Quaternary International, 244(1): 88-104.

Mieszkowska, N., Hawkins, S., Burrows, M., Kendall, M., 2007. Long-term changes in the geographic distribution and population structures of *Osilinus lineatus* (Gastropoda: Trochidae) in Britain and Ireland. Journal of the Marine Biological Association of the United Kingdom, 87(02): 537-545.

Milano, S., Schöne, B.R., Witbaard, R., 2017. Changes of shell microstructural characteristics of Cerastoderma edule (Bivalvia) — A novel proxy for water temperature. Palaeogeography, Palaeoclimatology, Palaeoecology, 465, Part B: 395-406.

Milner, N., 2001. At the Cutting Edge: Using Thin Sectioning to Determine Season of Death of the European Oyster, *Ostrea edulis*. Journal of Archaeological Science, 28(8): 861-873.

Oschmann, W., 2009. Sclerochronology: editorial. International Journal of Earth Sciences, 98(1): 1-2.

Prendergast, A.L., Azzopardi, M., O'Connell, T.C., Hunt, C., Barker, G., Stevens, R.E, 2013. Oxygen isotopes from Phorcus (Osilinus) turbinatus shells as a proxy for sea surface temperature in the central Mediterranean: A case study from Malta. Chemical Geology, 345: 77-86.

Prendergast, A.L., Stevens, R.E., O'Connell, T.C., Fadlalak, A., Touati, M., al-Mzeine, A., Schöne, B.R., Hunt, C.O., Barker, G., 2016. Changing patterns of eastern Mediterranean shellfish exploitation in the Late Glacial and Early Holocene: Oxygen isotope evidence from gastropod in Epipaleolithic to Neolithic human occupation layers at the Haua Fteah cave, Libya. Quaternary International, 407, Part B(Part B): 80-93.

Regis, M.B., 1972. Étude comparée de la croissance des Monodontes (Gastéropodes Prosobranches) en Manche et le long des côtes Atlantiques et Meditérranéenes françaises. Journal of Molluscan Studies, Supplément 3: 259-267.

Reynolds, D.J., Richardson, C.A., Scourse, J.D., Butler, P.G., Hollyman, P., Román-González, A., Hall, I.R., 2017. Reconstructing North Atlantic marine climate variability using an absolutely-dated sclerochronological network. Palaeogeography, Palaeoclimatology, Palaeoecology, 465, Part B: 333-346.

Reza Mirzaei, M., Yasin, Z., Shau Hwai, A.T., 2014. Periodicity and shell microgrowth pattern formation in intertidal and subtidal areas using shell cross sections of the blood cockle, *Anadara granosa*. The Egyptian Journal of Aquatic Research, 40(4): 459-468.

Rofes, J., Garcia-Ibaibarriaga, N., Aguirre, M., Martínez-García, B., Ortega, L., Zuluaga, M. C.; Bailon, S., Alonso-Olazabal, A., Castaños, J., Murelaga, X., 2015. Combining Small-Vertebrate, Marine and Stable-Isotope Data to Reconstruct Past Environments. Scientific reports, 5: 14219.

Román-González, A., Scourse, J.D., Butler, P.G., Reynolds, D.J., Richardson, C.A., Peck, L.S., Brey, T., Hall, I. R., 2017. Analysis of ontogenetic growth trends in two marine Antarctic bivalves *Yoldia eightsi* and *Laternula elliptica*: Implications for sclerochronology. Palaeogeography, Palaeoclimatology, Palaeoecology, 465: 300-306.

Salas, A., Díaz, F., Re, A.D., Galindo-Sanchez, C.E., Sanchez-Castrejon, E., González, M., Licea, A.;, Sanchez-Zamora, A., Rosas, C., 2014. Preferred temperature, thermal tolerance, and metabolic response of *Tegula regina* (Stearns, 1892). Journal of Shellfish Research, 33(1): 239-246.

Sato, S. 1995. Spawning periodicity and shell microgrowth patterns of the venerid bivalve *Phacosoma japonicum* (Reeve, 1850). Palaios, 38, 61-72.

Schöne, B.R., 2008. The curse of physiology—challenges and opportunities in the interpretation of geochemical data from mollusk shells. Geo-Marine Letters, 28(5-6): 269-285.

Schöne, B., Tanabe, K., Dettman, D., Sato, S., 2003. Environmental controls on shell growth rates and $\delta^{18}O$ of the shallow-marine bivalve mollusk *Phacosoma japonicum* in Japan. Marine Biology, 142(3): 473-485.

Schöne, B.R., Freyre Castro, A.D., Fiebig, J., Houk, S.D., Oschmann, W., Kröncke, I., 2004. Sea surface water temperatures over the period 1884–1983 reconstructed from oxygen

isotope ratios of a bivalve mollusk shell (Arctica islandica, southern North Sea). Palaeogeography, Palaeoclimatology, Palaeoecology, 212(3–4): 215-232.

Schöne, B.R., Houk, S.D., Castro, A.D.F., Fiebig, J., Oschmann, W., Kröncke, I., Dreyer, W., Gosselck, F., 2005a. Daily growth rates in shells of *Arctica islandica*: assessing sub-seasonal environmental controls on a long-lived bivalve mollusk. PALAIOS, 20(1): 78-92.

Schöne, B.R., Dunca, E., Fiebig, J., Pfeiffer, M., 2005b. Mutvei's solution: an ideal agent for resolving microgrowth structures of biogenic carbonates. Palaeogeography, Palaeoclimatology, Palaeoecology, 228(1): 149-166.

Schöne, B.R., Rodland, D.L., Wehrmann, A., Heidel, B., Oschmann, W., Zhang, Z., Fiebig, J., Beck, L., 2007. Combined sclerochronologic and oxygen isotope analysis of gastropod shells (*Gibbula cineraria*, North Sea): life-history traits and utility as a high-resolution environmental archive for kelp forests. Marine Biology, 150(6): 1237-1252.

Straus, L.G., 2017. The Pleistocene–Holocene Transition in Cantabrian Spain: current reflections on culture change. Journal of Quaternary Science. DOI: 10.1002/jqs.2943

Surge, D., Wang, T., Gutierrez-Zugasti, I., Kelley, P.H., 2013. Isotope sclerochronology and season of annual growth line formation in limpet shells (*Patella vulgata*) from cold- and warm-temperate zones in the eastern North Atlantic. PALAIOS, 28(6): 386-393.

Twaddle, R.W., Ulm, S., Hinton, J., Wurster, C.M., Bird, M.I., 2016. Sclerochronological analysis of archaeological mollusc assemblages: methods, applications and future prospects. Archaeological and Anthropological Sciences, 8(2): 359-379.

Usabiaga, J.I., Sáenz, J., Valencia, V., Borja, Á., 2004. Climate and meteorology: variability and its influence on the Ocean. Oceanography and Marine Environment of the Basque Country. Elsevier Oceanography Series, 70: 75-95.

Wang, T., Surge, D., Mithen, S., 2012. Seasonal temperature variability of the Neoglacial (3300–2500 BP) and Roman Warm Period (2500–1600 BP) reconstructed from oxygen

isotope ratios of limpet shells (*Patella vulgata*), Northwest Scotland. Palaeogeography, Palaeoclimatology, Palaeoecology, 317–318(0): 104-113.

Williams, E.E., 1965. Growth and Distribution of *Monodonta Lineata* on a Rocky Shore in Wales. University College of Wales, Aberystwyth.

Williamson, P., Kendall, M.A., 1981. Population Age Structure and Growth of the Trochid *Monodonta Lineata* Determined From Shell Ring. Journal of the Marine Biological Association of the United Kingdom, 61(04): 1011-1026.

Yanes, Y., Gutiérrez-Zugasti, I., Delgado, A., 2012. Late-glacial to Holocene transition in northern Spain deduced from land-snail shelly accumulations. Quaternary Research, 78(2): 373-385.

Caption list

Figure 1: Location of the study area in Cantabria (northern Spain).

Figure 2: a) Modern specimens of *Phorcus lineatus*. Dashed lines indicate the cutting axis from which two halves were obtained for sclerochronological studies. Calcium carbonate samples were taken on the half with the apex. b) Growth patterns studies were performed on a 2 mm-thick section, which was cut from the second half of each shell (the one with shell aperture). c) Thick section showing the internal shell structure. The main layers (periostracum, calcite and aragonite) and microgrowth lines and increments were identified in the cross-sections. d) Thick-section after immersion in Mutvei´s solution. The arrow shows the direction of shell growth.

Figure 3: Stable oxygen isotope curves of a) LANO-61, b) LANO-63, c) LANO-65 and d) LANO-66. The last portions of shell growth are located in the left part of the chart. DOG: direction of growth.

Figure 4: Cross-sections of *Phorcus lineatus* showing large-scale accretionary units (a-d) and small-scale accretionary units (e). Large-scale accretionary units correspond to annual slowdown of growth. Calcite penetrates into the aragonite layer (a-b). Thinner and brighter

lines (c-d). For small-scale accretionary units two different patterns of microgrowth lines and increments were identified (e): one microgrowth increment and one microgrowth line represented a tidal cycle (circatidal increments) and two microgrowth increments and two microgrowth lines represented a lunar day (circalunidian increments).

Figure 5: Sclerochronology and temporal alignment of the last whorl of LANO-63. The portion of shell growth represented in the figure was deposited during August and September 2012. a) During that time, the shell underwent five spring tides (open circles: full moon; filled circles: new moon) and four neap tides (circles open to the left or right: first and last quarter moon, respectively). The black lines/curves show the location of largest spring tides every fourteen days. The maximum and minimum height reported for the tide cycle was 5 m during high tide and 0.7 m during low tide. The maximum and minimum difference between high tide and subsequent low tide was 4.3 m and 1.2 m, respectively. The thick-section exhibited a series of microgrowth lines and increments formed with different periodicity. The blue line on the tidal cycle shows the tidal height area where inhabited by *P. lineatus*. b) $\delta^{18}O_{shell}$ values were temporally aligned with daily predicted $\delta^{18}O_{shell}$, assigning each $\delta^{18}O_{shell}$ value to a variable number of days according to the number of tidal cycles covered by each sample spot. Therefore, a variable number of daily predicted $\delta^{18}O_{shell}$ were assigned to each $\delta^{18}O_{shell}$. $\delta^{18}O_{shell}$ values and predicted $\delta^{18}O_{shell}$ showed high correlation ($r^2 = 0.84$, p-value < 0.0001).

Figure 6: Temporal alignment of $\delta^{18}O_{shell}$ values in the shells a) LANO-61, b) LANO-63, c) LANO-65 and d) LANO-66. The calendar alignment was completed by using fortnightly and daily increments observed in cross-section. All $\delta^{18}O_{shell}$ series showed a high correlation with predicted $\delta^{18}O_{shell}$ from daily T_{meas} and $\delta^{18}O_{water}$.

Figure 7: Growth increment (µm) per day for a) LANO-61, b) LANO-63, c) LANO-65 and d) LANO-66. Growth rates were calculated from the distance between carbonate samples (600 µm) and taking into account the number of days assigned to each shell portion between two sampling spots. The colour labels on the X-axis represent winter (blue), spring (green), summer (red) and autumn (brown). The grey labels represent cessation/slowdown, determined by sclerochronological analysis. The arrows show the direction of shell growth. Growth rates during the most recently deposited shell portion (and hence during the end of their life span) are located in right part of the charts.

Figure 8: Temporal alignment of $T_{\delta 18O}$ from a) LANO-61, b) LANO-63, c) LANO-65 and d) LANO-66. $T_{\delta 18O}$ was calculated from $\delta^{18}O_{shell}$ and average $\delta^{18}O_{water}$. The grey labels represent growth cessation/slowdown, determined by sclerochronological analysis. Error bars were calculated from $\delta^{18}O_{water}$ variability that occurred during the day(s) in which the sampled shell portion was formed plus the analytical precision of the mass spectrometer for each $\delta^{18}O_{shell}$ value. In general terms, $T_{\delta 18O}$ followed the instrumental temperatures very well.

Table 1: Collection dates and measurements of the studied *P. lineatus* specimens, and oxygen isotope maxima/minima values.

Table 2: Differences between $T_{\delta 18O}$ and average T_{meas} during the day(s) assigned to each $\delta^{18}O_{shell}$ by the temporal alignment.

Table 3: Differences between maximum and minimum $T_{\delta 18O}$ from the four shells and maximum and minimum daily T_{meas}.

Table 1

ID Sample	Collection date	Collection season	Location	Size (mm)		Maximum $\delta^{18}O$ (VPDB ‰)	Minimum $\delta^{18}O$ (VPDB ‰)	Range (VPDB ‰)
				Length	Diameter			
LANO-61	10/1/2012	Autumn	Langre	14.2	15.8	2.08	-0.02	2.10
LANO-63	10/1/2012	Autumn	Langre	13.6	14.4	1.46	0.16	1.30
LANO-65	4/22/2012	Spring	Langre	16.1	17.2	2.22	0.42	1.80
LANO-66	4/22/2012	Spring	Langre	16.2	17.4	2.25	0.42	1.83
Mean				15.0	16.2	2.00	0.25	1.76
Standard Deviation (1 σ)				1.15	1.21	0.32	0.19	0.29

Table 2

Numer of sample	$T_{\delta 18O}$ (°C) from LANO-61	Average T_{meas} (°C) days of growth	Difference between $T_{\delta 18O}$ and T_{meas} (°C)	$T_{\delta 18O}$ (°C) from LANO-63	Average T_{meas} (°C) days of growth	Difference between $T_{\delta 18O}$ and T_{meas} (°C)	$T_{\delta 18O}$ (°C) from LANO-65	Average T_{meas} (°C) days of growth	Difference between $T_{\delta 18O}$ and T_{meas} (°C)	$T_{\delta 18O}$ (°C) from LANO-66	Average T_{meas} (°C) days of growth	Difference between $T_{\delta 18O}$ and T_{meas} (°C)
1	17.9	17.6	+0.3	17.9	19.5	-1.6	12.4	12.9	-0.5	13.2	13.9	-0.6
2	18.1	18.9	-0.7	16.4	17.3	-0.8	12.6	13.7	-1.1	13.2	13.4	-0.2
3	20.7	20.9	-0.3	16.3	16.4	-0.1	13.0	12.8	+0.3	13.3	13.1	+0.3
4	20.0	20.5	-0.5	17.5	19.5	-2.0	12.6	12.5	+0.1	12.2	12.0	+0.2
5	20.7	21.2	-0.6	18.9	19.4	-0.5	13.4	11.7	+1.7	11.5	11.8	-0.3
6	20.8	21.7	-1.0	19.9	20.7	-0.8	11.7	11.5	+0.2	14.0	14.5	-0.5
7	22.0	21.1	+0.8	19.4	20.1	-0.7	13.0	13.5	-0.5	16.6	15.2	1.4
8	22.3	22.0	+0.2	20.2	21.2	-1.0	14.9	14.8	+0.1	15.4	15.3	+0.2
9	22.5	22.3	+0.2	20.8	21.3	-0.5	16.2	15.9	+0.3	15.8	16.1	-0.3
10	21.1	20.8	+0.2	21.6	22.9	-1.4	16.1	16.5	-0.3	15.4	16.5	-1.1
11	20.6	20.9	-0.3	21.3	21.7	-0.4	17.0	17.0	0.0	16.8	16.8	0.0
12	20.4	20.7	-0.2	21.2	20.8	+0.3	17.9	16.9	+1.0	17.7	17.1	+0.7
13	20.2	19.2	+1.0	20.4	21.0	-0.6	17.4	16.8	+0.7	19.5	19.7	-0.2
14	19.5	19.4	+0.0	20.1	20.3	-0.2	18.7	18.1	+0.6	19.1	19.4	-0.3
15	18.2	18.1	+0.1	20.7	19.7	+1.0	19.5	19.9	-0.4	18.7	19.5	-0.8
16	17.2	17.3	-0.1	19.6	19.8	-0.2	19.5	19.6	-0.1	19.0	18.3	+0.7
17	16.9	16.7	+0.2	17.8	18.2	-0.3	18.4	18.2	+0.2	18.0	18.4	-0.4
18	15.1	15.4	-0.3	17.9	18.1	-0.3	16.5	16.8	-0.3	15.6	15.5	+0.1
19	13.5	13.8	-0.3	17.3	17.3	0.0	15.5	15.4	0.0	14.9	15.2	-0.3
20	12.5	13.6	-1.1	17.1	17.3	-0.2	13.5	13.8	-0.3	13.4	13.6	-0.2
21	12.8	13.1	-0.3	16.8	16.9	-0.1	12.1	12.8	-0.8	13.2	13.0	+0.2
22	13.0	13.6	-0.5	16.4	16.1	+0.3	11.1	11.7	-0.6	11.3	12.5	-1.3
23	13.4	13.9	-0.5	15.9	15.5	+0.4	11.7	12.9	-1.2	11.0	11.6	-0.7
24	13.8	13.2	+0.6	15.5	15.4	+0.2	11.6	12.5	-0.9	11.9	12.4	-0.5

25	13.2	12.9	+0.3	14.8	14.5	+0.3	12.0	12.5	-0.5	15.4	14.8	+0.6
26	13.3	13.1	+0.2	14.7	14.7	+0.0	14.2	13.7	+0.5	15.3	15.4	-0.1
27	12.8	12.6	+0.2	13.1	13.3	-0.1	15.5	15.5	0.0	15.4	15.5	-0.1
28	12.4	12.3	+0.1	13.5	13.3	+0.2	15.7	16.1	-0.4	14.5	16.1	-1.5
29	12.0	11.8	+0.2	13.1	13.0	+0.1	15.7	16.8	-1.0	14.8	17.0	-2.2
30	11.6	11.8	-0.1	13.3	13.2	+0.2	14.7	16.4	-1.7	14.0	16.4	-2.5
31	12.3	12.4	+0.0				14.4	16.3	-1.9	14.1	16.9	-2.8
32	13.2	13.1	+0.1				15.0	17.5	-2.5	16.2	17.1	-0.9
33	13.5	13.7	-0.2				16.5	18.3	-1.7	16.7	18.0	-1.3
34	13.4	13.5	-0.1				14.6	17.2	-2.6	16.3	18.3	-2.0
35	14.0	13.8	+0.2				16.8	17.9	-1.0	15.9	16.8	-0.9
36	14.4	14.5	-0.1				16.5	17.8	-1.3	16.8	17.6	-0.8
37	15.4	15.0	+0.4									
38	14.5	14.6	-0.2									
39	15.1	15.0	+0.1									
Mean	16.3	16.3	0.3	17.7	17.9	0.5	14.9	15.4	0.7	15.2	15.7	0.8
Maximum	22.5	22.3	1.0	21.6	22.9	1.0	19.5	19.9	1.7	19.5	19.7	1.4
Minimum	11.6	11.8	-1.1	13.1	13.0	-2.0	11.1	11.5	-1.7	11.0	11.6	-2.5
Range	10.9	10.6	2.1	8.4	9.9	3.0	8.4	8.4	3.4	8.5	8.1	3.9

Table 3

ID Sample	Maximum $T_{\delta^{18}O}$ (°C)	Maximum T_{meas} (°C)	Difference with Maximum T_{meas} (°C)	Minimum $T_{\delta 18O}$ (°C)	Minimum T_{meas} (°C)	Difference with Minimum T_{meas} (°C)
LANO-61	22.5	23.1	-0.6	11.6	11.1	+0.5
LANO-63	21.6	23.1	-1.5	13.1	11.1	+2.0
LANO-65	19.5	21.5	-2.0	11.1	11.1	+0.0
LANO-66	19.5	21.5	-2.0	11.0	11.1	+0.1

1. Spanish Institute of Oceanography

2. Langre beach

Figure 1

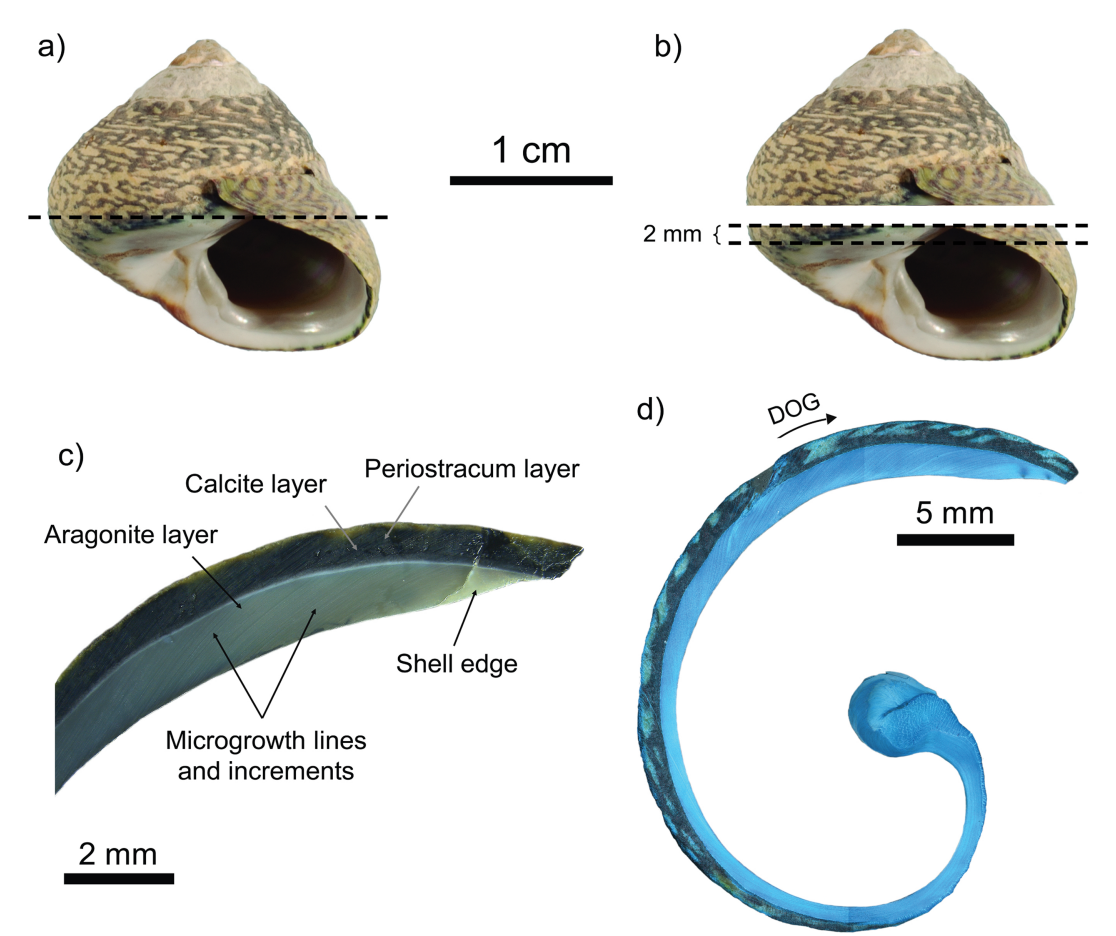
a)
1 cm
b)
2 mm
c)
Calcite layer
Periostracum layer
Aragonite layer
Shell edge
Microgrowth lines
and increments
2 mm
d)
DOG
5 mm

Figure 2

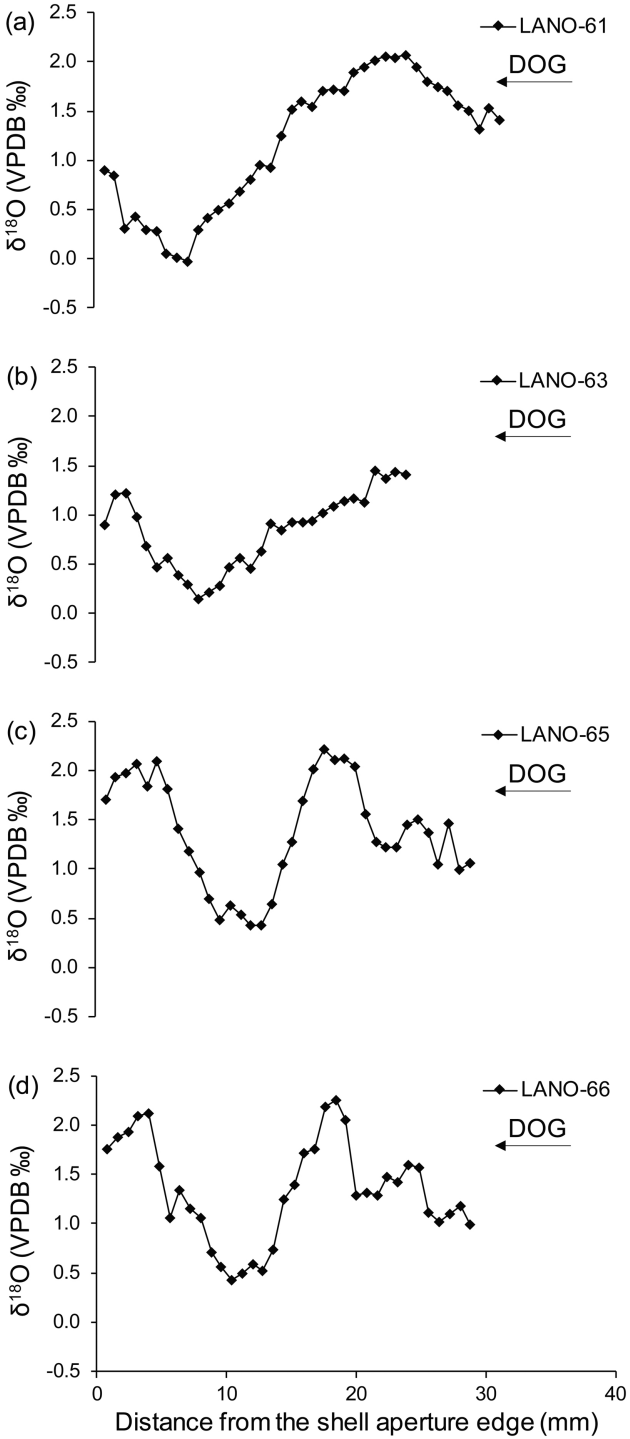
(a)
LANO-61
DOG
(b)
LANO-63
DOG
(c)
LANO-65
DOG
(d)
LANO-66
DOG
δ18O (VPDB ‰)
2.5
2.0
1.5
1.0
0.5
0.0
-0.5
0
10
20
30
40
Distance from the shell aperture edge (mm)

Figure 3

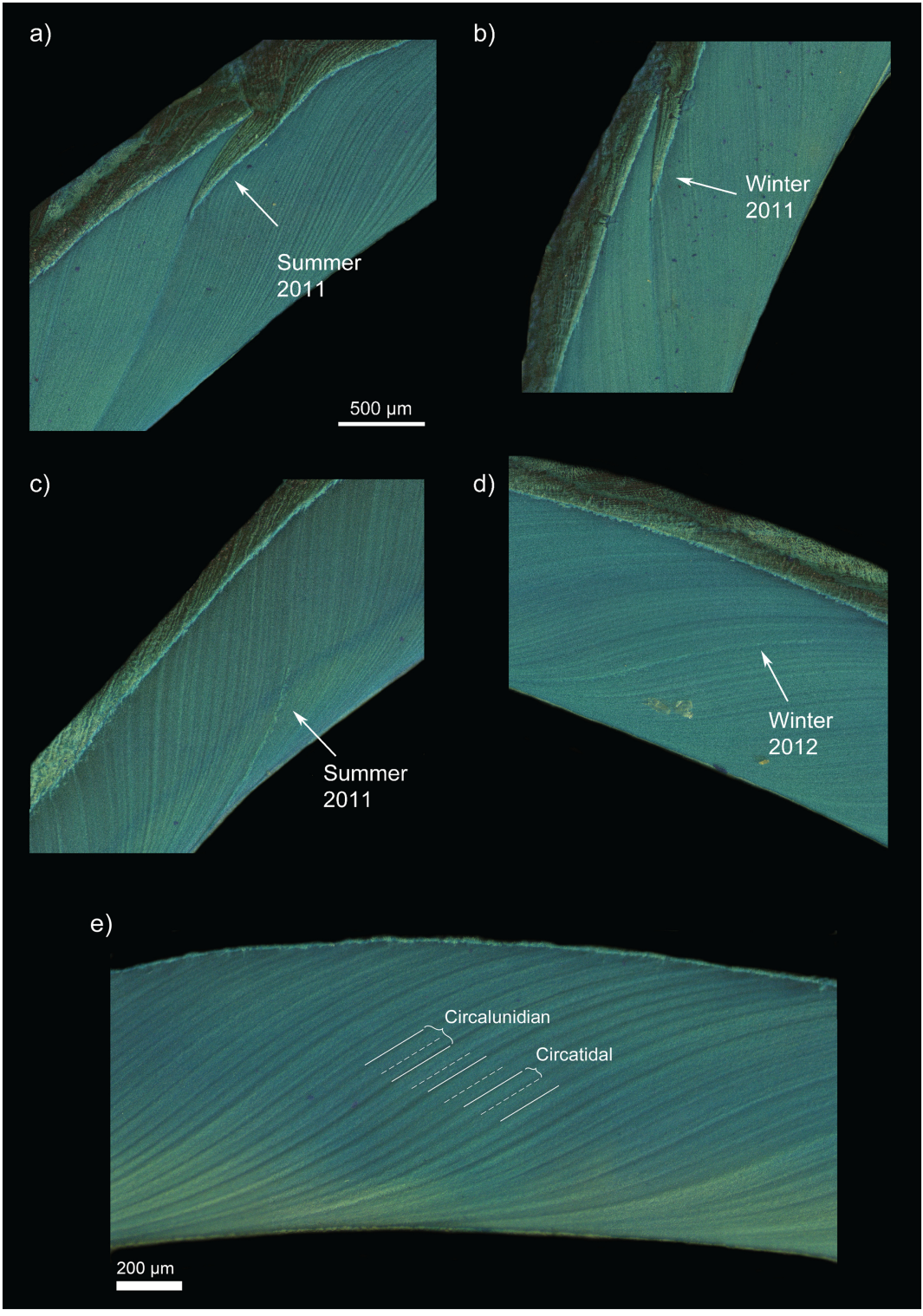
a)
Summer
2011
500 µm
b)
Winter
2011
c)
Summer
2011
d)
Winter
2012
e)
Circalunidian
Circatidal
200 µm

Figure 4

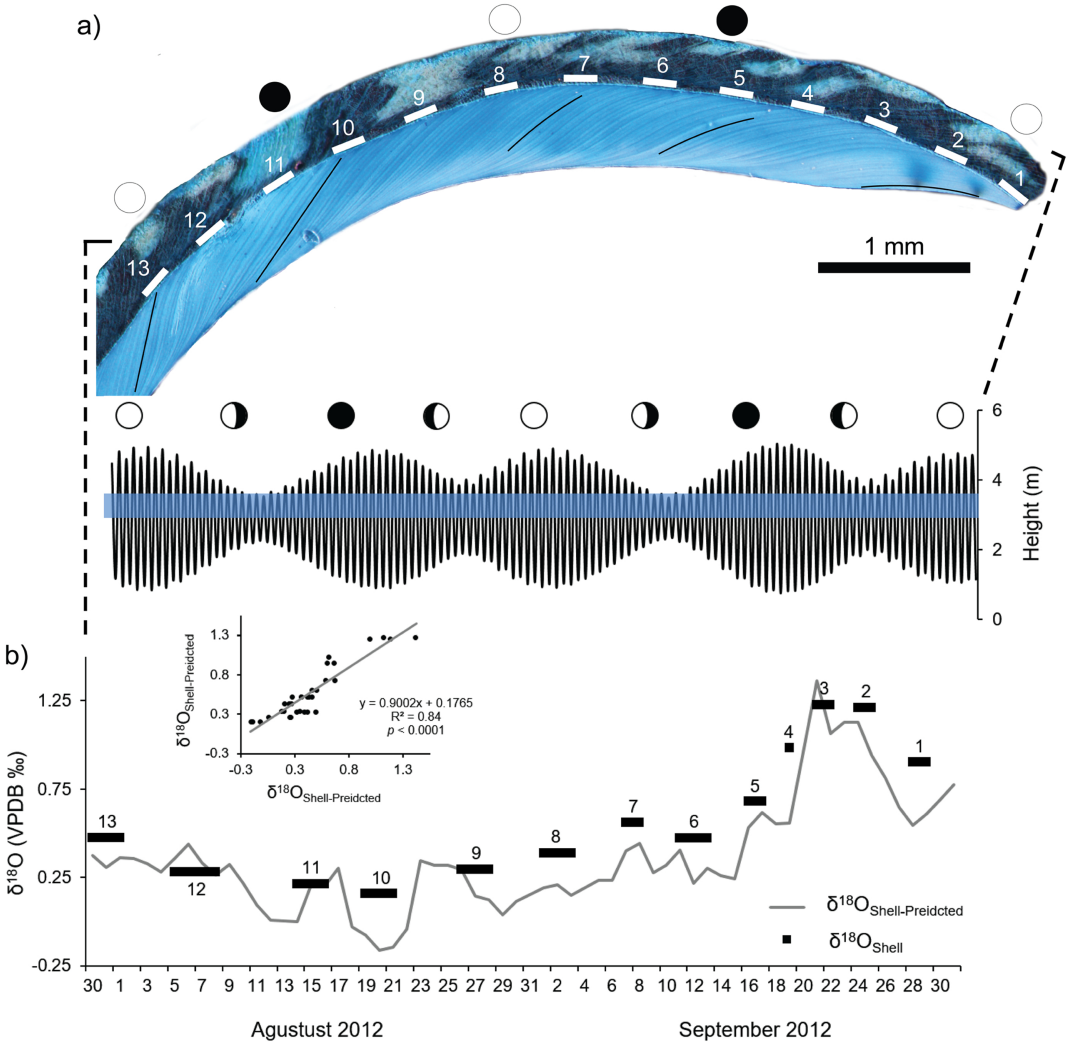
a)
1
2
3
4
5
6
7
8
9
10
11
12
13
1 mm
Height (m)
0
2
4
6
b)
δ18O (VPDB ‰)
1.25
0.75
0.25
-0.25
δ18OShell-Preidcted
δ18OShell
y = 0.9002x + 0.1765
R² = 0.84
p < 0.0001
δ18OShell-Preidcted
δ18OShell
30 1 3 5 7 9 11 13 15 17 19 21 23 25 27 29 31 2 4 6 8 10 12 14 16 18 20 22 24 26 28 30
Agustust 2012
September 2012

Figure 5

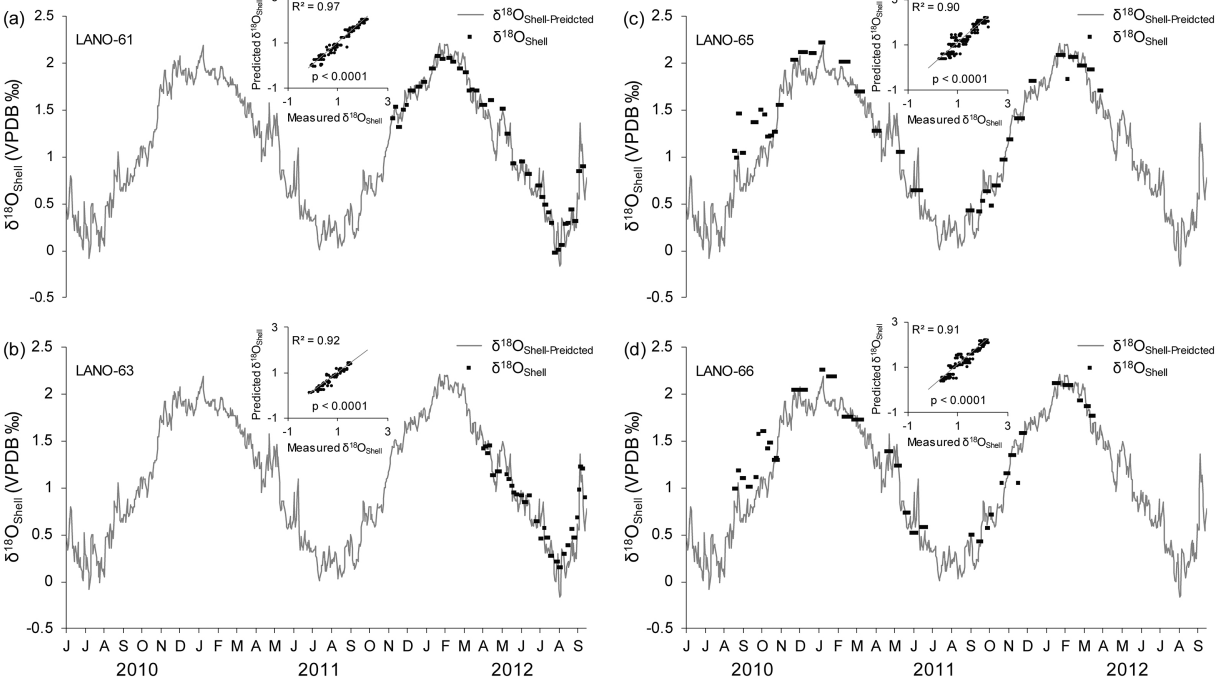
(a)
LANO-61
R² = 0.97
p < 0.0001
Predicted δ18OShell
Measured δ18OShell
δ18OShell-Preidcted
δ18OShell
δ18OShell (VPDB ‰)
(b)
LANO-63
R² = 0.92
p < 0.0001
(c)
LANO-65
R² = 0.90
p < 0.0001
(d)
LANO-66
R² = 0.91
p < 0.0001
J J A S O N D J F M A M J J A S O N D J F M A M J J A S
2010
2011
2012

Figure 6

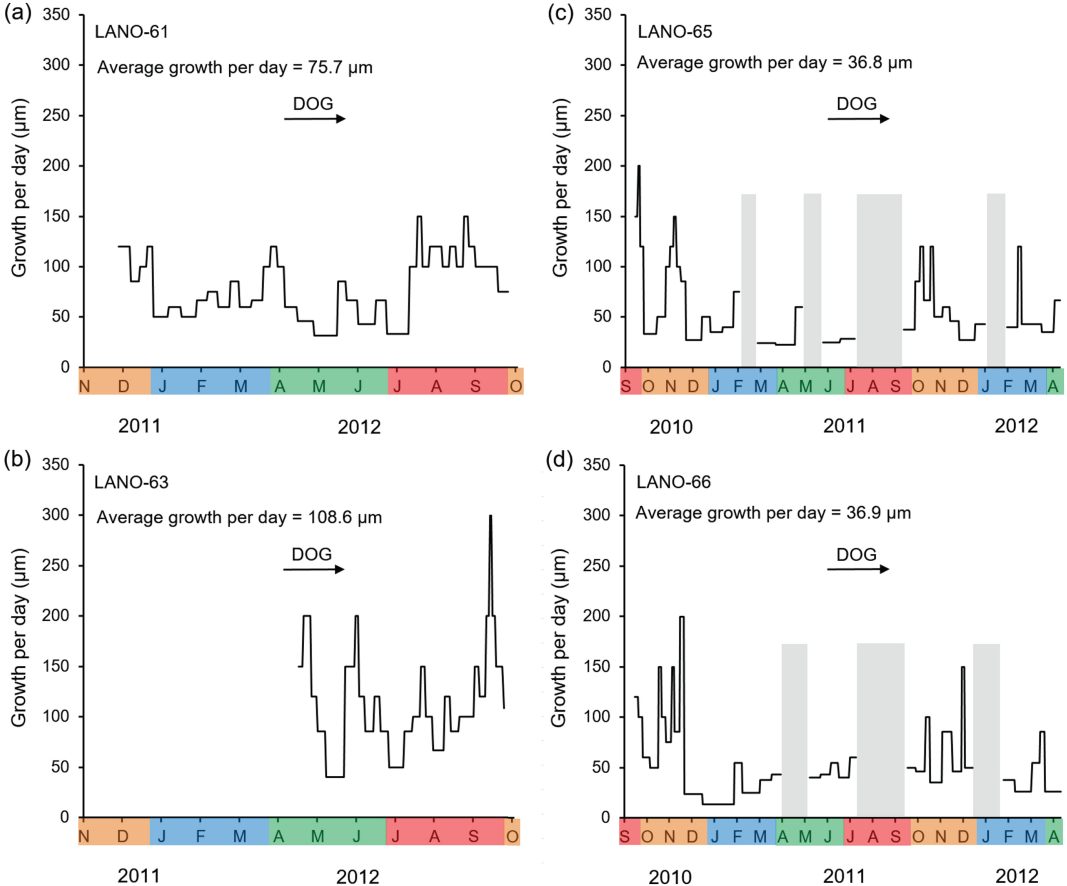
(a)
LANO-61
Average growth per day = 75.7 µm
DOG
Growth per day (µm)
350
300
250
200
150
100
50
0
N D J F M A M J J A S O
2011
2012
(c)
LANO-65
Average growth per day = 36.8 µm
DOG
Growth per day (µm)
S O N D J F M A M J J A S O N D J F M A
2010
2011
2012
(b)
LANO-63
Average growth per day = 108.6 µm
DOG
Growth per day (µm)
N D J F M A M J J A S O
2011
2012
(d)
LANO-66
Average growth per day = 36.9 µm
DOG
Growth per day (µm)
S O N D J F M A M J J A S O N D J F M A
2010
2011
2012

Figure 7

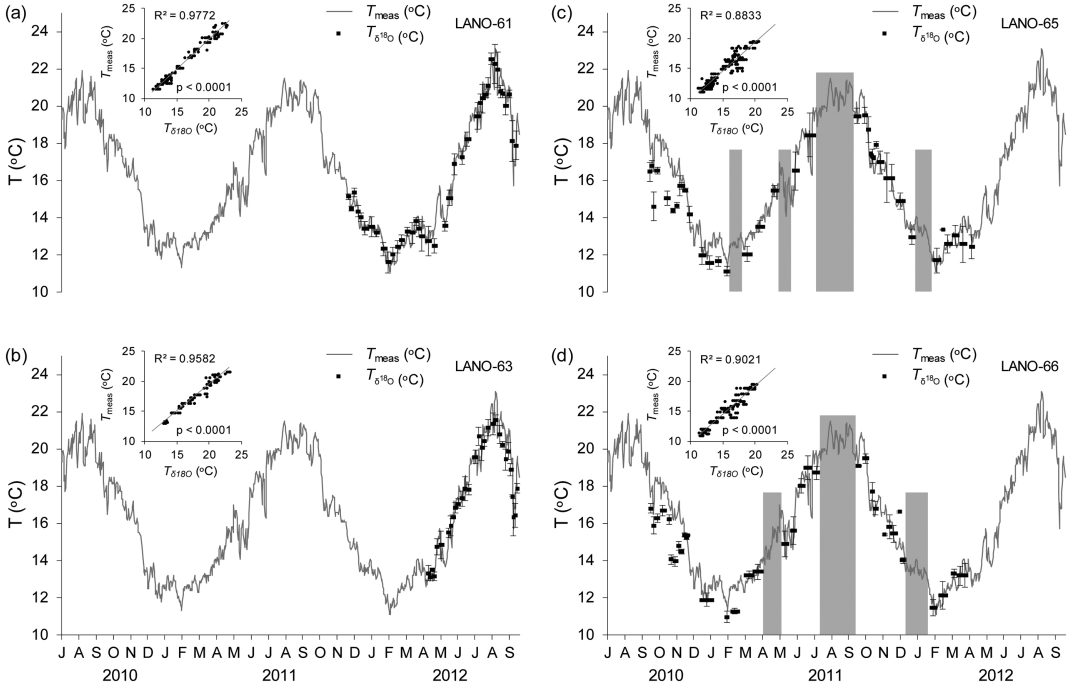
(a)
LANO-61
T_{meas} (°C)
$T_{\delta 18O}$ (°C)
R² = 0.9772
p < 0.0001
T_{meas} (°C)
$T_{\delta 18O}$ (°C)
T (°C)
(b)
LANO-63
R² = 0.9582
p < 0.0001
(c)
LANO-65
R² = 0.8833
p < 0.0001
(d)
LANO-66
R² = 0.9021
p < 0.0001
J A S O N D J F M A M J J A S O N D J F M A M J J A S
2010
2011
2012

Figure 8